

An Efficient Solution Method for Buoyancy-Wave Equation at Variable Wind and Temperature

Rein Rõõm*, Marko Zirk

Tartu University, Estonia

Corresponding author address:

Rein Rõõm, Institute of Environmental Physics, Tartu University.

Ülikooli 18, Tartu 50090, Estonia.

E-mail: Rein.Room@ut.ee

Abstract

To solve a horizontally spectral, vertically discrete buoyancy wave equation in conditions of arbitrary wind and temperature distribution with height, the solution factorization method is applied, which consists in presentation of solution in the form of a cumulative product of complex decrease factors. For decrease factors a nonlinear, inhomogeneous, two-member recurrence formula follows, which is initiated, assuming the topmost discrete layer of the atmosphere to be inviscid and homogeneously stratified, in which case the initial decrease factor can be uniquely determined from radiative condition. Singularities in the wave equation, corresponding to a critical layer in the vicinity of evanescent wind, are eliminated by turbulent friction. Estimation of minimal vertical resolution, enabling solution stability and accuracy, is derived. The area of application of the developed numerical scheme is high resolution, high precision modeling of orographic waves for arbitrary orography in complex atmospheric stratification conditions. Solution can be applied also for testing of adiabatic kernels of numerical weather prediction models.

1 Introduction

When examining the models and methods used for buoyancy wave studies, two main groups may be disposed: (i) The linear analytical approach (Queney 1948, Scorer 1949, Wurtele 1957, Crapper 1959, 1962, Jones 1967, Berkshire 1975, Gjevik and Marthinsen 1978, Smith 1980, 1988, 1989a,b, Janovich 1984, Phillips 1984, Sharman and Wurtele 1983, 2004, Broad 1995, 1999, Pinty et al 1995, Shutts 1995, 1998, 2003, Grubišić and Smolarkiewicz 1997, Saito et al 1998, Rõõm and Männik 1999, Welch and Smolarkiewicz 2001, Broutman et al 2003, Männik et al 2003, Polvani et al 2004); (ii) Nonlinear, finite difference method (Long 1953, 1954, Drazin and More 1967, Miles 1968a, b, Miles and Huppert 1969, Clark 1977, Klemp and Lilly 1978, Durran and Klemp, 1983, Laprise and Peltier 1989, Wurtele et al 1987, 1996, Xue and Thorpe 1991, Miranda and James 1992, Rottman et al 1996, Miranda and Valente 1997, Nance and Durran 1997, 1998, Holton and Alexander 1999, Rõõm et al 2001, Teixeira and Miranda 2004, Rõõm et al 2006). Advantages of the linear analytical approach are the high spatial and temporal resolution, a possibility to study the stationary and transient regimes in separation, and the existence of analytical means for stability etc. analysis. The main disadvantage is the restriction to simplest ('analytical') flow regimes (like the linear shear or constant stability). Benefit of finite difference trend lies in base-state generality, which supports realistic experimental conditions. The main disadvantages are the moderate spatial resolution and inability to

treat the steady and transient regimes separately.

In this paper, a novel method for solution of linear buoyancy wave equation is presented, which combines the best of both approaches, being linear and (maximum possible) analytical, and at the same time, numerical, accepting arbitrary vertical distributions of reference wind and temperature. The algorithm proves effective and fast as it makes use of direct computation of the decrease factors via a straightforward recurrence formula, whose initial value is specified from the radiative condition at the top. The cumulative product of decrease factors from bottom to top yields a solution for omega-velocity with the precision of a constant factor, the value of which can be specified from bottom boundary condition. Thus, solution of wave equation will take very little effort and the major computational time goes to preparation of equation coefficients and summation of obtained orthogonal modes over wave numbers to get the solution in ordinary physical coordinates. Also, the numerical solution has clear physical content, as the modulus of a complex decrease factor presents the actual decrease of the wave amplitude per single layer of discrete model, whereas its argument is the phase angle increment per layer.

As the model deals with variable winds, there a problem arises inevitably with critical wave-vectors and critical levels, corresponding to singularities in wave equation. This problem is solved in the current numerical approach with inclusion of turbulent friction into forcing, yielding singularity removing. The use of turbulent viscosity for wave-equation regularization purpose was

proposed already by Lin (1955), Jones (1967), and Hazel (1967). However, the theoretical estimates of maximum stable vertical grid-step will show, that the requirements to high vertical resolution remain, especially in the vicinity of critical levels. This is the point where the numerical efficiency of the method becomes crucial, enabling application of sufficiently high spatial resolution where appropriate.

Though there exist various 'ready' wave equations, they do differ, depending on the 'small' details of initial dynamical model, like the used coordinate frames etc, rather substantially in appearance. To avoid potential ambiguities in initial definitions, we start with a short introduction of the wave equation which is used in this investigation, from MPW model (a certain non-hydrostatic, semi-elastic pressure-coordinate model, developed by Miller 1974, Miller and Pearce 1974, Miller and White 1984, and White 1989).

2 Continuous spectral wave equation

When using the non-dimensional log-pressure coordinate $\zeta = \ln(p_0/p)$, $\Rightarrow p = p_0 e^{-\zeta}$, ($p_0 = 1000hPa$ is the mean sea-level pressure) instead of the common pressure p , the linearised version (R  m 1998) of the MPW model reads

$$\left(\frac{\partial}{\partial t} + \mathbf{U} \cdot \nabla\right) \omega = -R \frac{p}{H^2} T + \frac{p}{H^2} \frac{\partial \varphi}{\partial \zeta} + \gamma \nabla^2 \omega, \quad (1a)$$

$$\left(\frac{\partial}{\partial t} + \mathbf{U} \cdot \nabla\right) \mathbf{v} = \mathbf{U}' \frac{\omega}{p} - \nabla \varphi - \mathbf{f} \times \mathbf{v} + \gamma \nabla^2 \mathbf{v}, \quad (1b)$$

$$\left(\frac{\partial}{\partial t} + \mathbf{U} \cdot \nabla\right) T = \theta \frac{\omega}{p} + \gamma \nabla^2 T, \quad (1c)$$

$$\nabla \cdot \mathbf{v} - \frac{\partial \omega}{p \partial \zeta} = 0. \quad (1d)$$

Dynamic fields are the omega-velocity $\omega = Dp/Dt$ (with D/Dt as the material derivative), temperature fluctuation T , nonhydrostatic geopotential fluctuation φ , and horizontal velocity fluctuation \mathbf{v} . Reference (background) state of the atmosphere is presented by stationary, horizontally homogeneous wind vector $\mathbf{U}(\zeta)$ with $\mathbf{U}' = \partial \mathbf{U} / \partial \zeta$, background temperature $T^0(\zeta)$, gas constant of dry air R , and constant Coriolis parameter $f = |\mathbf{f}|$ where \mathbf{f} is a vertical vector. The scale height H and the stability parameter θ are

$$H(\zeta) = \frac{RT^0(\zeta)}{g}, \quad \theta(\zeta) = \frac{R}{c_p} T^0(\zeta) + \frac{\partial T^0}{\partial \zeta},$$

$\gamma = \gamma(\zeta)$ is the height-dependent kinematical turbulent viscosity coefficient.

Applying to dynamic fields Fourier presentation

$$\{T, \omega, u, v, \varphi\} = \sum_{\mathbf{k}} \left\{ \hat{T}_{\mathbf{k}}, \hat{\omega}_{\mathbf{k}}, \hat{u}_{\mathbf{k}}, \hat{v}_{\mathbf{k}}, \hat{\varphi}_{\mathbf{k}} \right\} e^{i(\mathbf{k} \cdot \mathbf{x} - \nu_{\mathbf{k}}^0 t)},$$

where amplitudes $\hat{T}_{\mathbf{k}}, \hat{\omega}_{\mathbf{k}}, \hat{u}_{\mathbf{k}}, \hat{v}_{\mathbf{k}}, \hat{\varphi}_{\mathbf{k}}$ are functions of ζ , \mathbf{k} is the wave-vector and $\nu_{\mathbf{k}}^0$ is the corresponding eigen-frequency, system (1) transforms to spectral normal-mode equations

$$i\nu \hat{\omega}_{\mathbf{k}} = -R \frac{p}{H^2} \hat{T}_{\mathbf{k}} + \frac{p}{H^2} \frac{\partial \hat{\varphi}_{\mathbf{k}}}{\partial \zeta}, \quad (2a)$$

$$i\nu \hat{\mathbf{v}}_{\mathbf{k}} = \mathbf{U}' \frac{\hat{\omega}_{\mathbf{k}}}{p} - i\mathbf{k} \hat{\varphi}_{\mathbf{k}} - \mathbf{f} \times \hat{\mathbf{v}}_{\mathbf{k}}, \quad (2b)$$

$$i\nu \hat{T}_{\mathbf{k}} = \theta \frac{\hat{\omega}_{\mathbf{k}}}{p}, \quad (2c)$$

$$i\mathbf{k} \cdot \hat{\mathbf{v}}_{\mathbf{k}} - \frac{\partial \hat{\omega}_{\mathbf{k}}}{p \partial \zeta} = 0, \quad (2d)$$

where

$$\nu = \mathbf{U}(\zeta) \cdot \mathbf{k} - \nu_{\mathbf{k}}^0 + i\gamma(\zeta)k^2 \quad (2e)$$

is the intrinsic frequency or eigen-frequency. Eigen-frequency is complex in presence of turbulent viscosity, which will produce weakening of free orthogonal modes in time, or, in the case of stationary solution, down-stream and upward weakening of wave amplitude in comparison with the friction-free case.

It is straightforward to derive from (2) a single scalar equation for the spectral

amplitude of omega velocity (short notation $\omega = \hat{\omega}_{\mathbf{k}}$ is used in following)

$$\alpha \frac{\partial}{\partial \zeta} \frac{1}{\alpha} \frac{\partial \omega}{\partial \zeta} - \beta \frac{\partial \omega}{\partial \zeta} + \lambda \omega = 0, \quad (3)$$

where coefficients, which are functions of ζ , are as follows

$$\alpha = \frac{p\nu}{\nu^2 - f^2}, \quad \beta = \frac{\nu\rho + \mathbf{i}f\tau}{\nu^2 - f^2}, \quad \lambda = k^2 H^2 \frac{N^2 - \nu^2}{\nu^2 - f^2} - \alpha \frac{\partial}{\partial \zeta} \frac{\nu\rho + \mathbf{i}f\tau}{p\nu}$$

$$\rho = \mathbf{k} \cdot \mathbf{U}', \quad \tau = U'_x k_y - U'_y k_x.$$

The bottom and top boundary conditions for this equation are

$$\omega(0) = \mathbf{i}\mathbf{k} \cdot \mathbf{U}(0) p_{\mathbf{k}}(0), \quad \lim_{\zeta \rightarrow \infty} |\omega| (p_0/p)^{1/2} = \lim_{\zeta \rightarrow \infty} |\omega| e^{\zeta/2} = 0. \quad (4)$$

The first one presents free slip condition. The second, top boundary condition, used here, is more restrictive in comparison with the condition $\lim_{\zeta \rightarrow \infty} |\omega| = 0$, commonly applied in numerical models, yet the more correct one, providing finiteness of kinetic energy, associated with vertical velocity $w = -H\omega/p$.

In the case of uniform velocity $U'_x, U'_y = 0$, $\Rightarrow \rho, \tau, \beta = 0$, $\nu = \text{const.}$, equation (3) simplifies to

$$\omega'' + \omega' + \lambda \omega = 0, \quad \lambda = k^2 H^2 \frac{N^2 - \nu^2}{\nu^2 - f^2}. \quad (3')$$

If, in addition, H, N are constants and the atmosphere is friction-free, $\gamma = 0$, then λ is a real constant. In this particular case, the analytic solution of (3'),

satisfying top boundary condition in (4) and the wave group energy upward propagation requirement (the radiative top condition, see Baines, 1995), is

$$\omega = \begin{cases} e^{-(1/2+\sqrt{1/4-\lambda})\zeta}, \lambda < 1/4, \\ e^{(-1/2+i\sqrt{\lambda-1/4})\zeta}, \lambda > 1/4. \end{cases} \quad (5)$$

If the atmosphere is topped by a homogeneous inviscid layer, solution (5) holds there. This property we shall use to formulate the upper boundary condition for discrete model.

3 Discrete spectral buoyancy-wave equation

Let us introduce a staggered vertical grid with full levels ζ_i , and half levels $\zeta_{i+1/2}$,

$$0 = \zeta_{1/2} < \zeta_1 < \dots < \zeta_{i-1} < \zeta_{i-1/2} < \zeta_i < \zeta_{i+1/2} < \dots < \zeta_M < \zeta_{M+1/2} < \infty,$$

where M is the number of discrete layers. Layer are centered at ζ_i and layer boundaries are at levels $\zeta_{i\pm 1/2}$. Discrete omega field is located on half-levels: $\omega_{i+1/2}$, whereas differences are located on full levels:

$$\Delta\omega_i = \omega_{i+1/2} - \omega_{i-1/2}.$$

Auxiliary functions $\rho, \tau, \alpha, \beta, \lambda$ are considered analytical functions of ζ and thus, defined for each $\zeta_i, \zeta_{i+1/2}$ analytically.

The discrete approximation of (3) is

$$L_{i+1/2}^+ \Delta\omega_{i+1} - L_{i+1/2}^- \Delta\omega_i + \Delta\zeta_{i+1/2}^2 \lambda_{i+1/2} \omega_{i+1/2} = 0, \quad (6)$$

with coefficients

$$L_{i+1/2}^+ = \frac{\Delta\zeta_{i+1/2}}{\Delta\zeta_{i+1}} \left(\frac{\alpha_{i+1/2}}{\alpha_{i+1}} - \frac{1}{2} \Delta\zeta_{i+1/2} \beta_{i+1/2} \right),$$

$$L_{i+1/2}^- = \frac{\Delta\zeta_{i+1/2}}{\Delta\zeta_i} \left(\frac{\alpha_{i+1/2}}{\alpha_i} + \frac{1}{2} \Delta\zeta_{i+1/2} \beta_{i+1/2} \right).$$

where $\Delta\zeta_i = \zeta_{i+1/2} - \zeta_{i-1/2}$, $\Delta\zeta_{i+1/2} = \zeta_{i+1} - \zeta_i$. The bottom and top boundary conditions (4) become in the discrete case

$$\omega_{1/2} = \mathbf{ik} \cdot \mathbf{U}_{1/2} p_{\mathbf{k},1/2}, \quad \lim_{\zeta_M \rightarrow \infty} |\omega_{M+1/2}| e^{\zeta_M/2} < \infty. \quad (7)$$

The top condition here does not insist on exact zero at any finite top height ζ_M , as this would cause spurious wave reflections on the top, but requires an asymptotic zero limit at $M \rightarrow \infty$. In more detail the content of this condition will be opened below.

4 Solution factorization technique

Considering tentatively the i th layer homogeneous and friction-free, solution in this layer presents in the exponential form (5), allowing to define the

decrease factor of ω in the layer as

$$c_i \equiv e^{\chi_i \Delta \zeta_i} = \frac{\omega_{i+1/2}}{\omega_{i-1/2}},$$

where χ_i is the (complex) phase shift in the layer of unit depth. The solution can be presented on discrete half-levels as a cumulative product of decrease factors

$$\omega_{i+1/2} = \omega_{1/2} \prod_{j=1}^i c_j, \quad j = 1, 2, \dots, M, \quad (8)$$

with $\omega_{1/2}$, defined in (7). In the general non-homogeneous case, we will seek solution in the same form (8), though the layers are not homogeneous anymore (moreover, presentation (8) does not need such a restrictive precondition but supports instead an assumption of continuous and differentiable altering of reference atmosphere inside layers). Loading (8) into wave equation (6) yields a two-point, nonlinear, non-homogeneous recurrence for c_i

$$L_{i+1/2}^+(c_{i+1} - 1) + L_{i+1/2}^-(1/c_i - 1) + \Delta \zeta_{i+1/2}^2 \lambda_{i+1/2} = 0. \quad (9)$$

As it proves, the recurrence direction is an essential property here. Recurrence (9) is stable for course from top to bottom, in direction of decreasing k and increasing ω , and it proves unstable for opposite direction, if the top condition in (7) is applied, as ω is exponentially decreasing with height by absolute value. For application of recurrence (9), one has to know the top start value c_M . To get c_M , it is advantageous to study the homogeneous

sub-case at first.

4.1 Special case of homogeneous inviscid atmosphere

Homogeneous stratification in a discrete model assumes both the homogeneous background state and homogeneous layering

$$\mathbf{U} = \mathbf{const.}, \quad T^0, N = \text{const.}, \quad \Delta\zeta_i = \Delta\zeta_{i+1/2} = \Delta\zeta. \quad (10)$$

In this case $\beta_{i+1/2} = 0$, while L^\pm and λ in (6) become height-independent

$$L_{i+1/2}^\pm = L^\pm = e^{\pm\Delta\zeta/2}, \quad \lambda_{i+1/2} = \lambda = H^2 k^2 \frac{N^2 - \nu^2}{\nu^2 - f^2}.$$

Considering the friction-free atmosphere, $\gamma = 0$, and stationary solution $\nu_{\mathbf{k}}^0 = 0$, we will have $\nu = \mathbf{k} \cdot \mathbf{U}$, i.e., λ becomes a real constant. To the homogeneous continuous solution (5), in the discrete, homogeneous, friction-free model, index-independent decrease factors correspond

$$c_i = c, \quad (11)$$

resulting in reduction of general recurrence (9) to a quadratic equation for c , identical for each i th level:

$$e^{\Delta\zeta/2}(c - 1) + e^{-\Delta\zeta/2}(c^{-1} - 1) + (\Delta\zeta)^2 \lambda = 0.$$

Solutions of this equation depend on the parameter

$$Q = \cosh(\Delta\zeta/2) - \frac{1}{2}(\Delta\zeta)^2\lambda. \quad (12)$$

There exists three regions: $Q \leq -1$, $-1 < Q < 1$, and $Q \geq 1$ with different behavior of solution. For $Q \leq -1$ the physically meaningful solution does not exist. This indicates, that $\Delta\zeta$ is chosen too large and should be reduced, because $\lim_{\Delta\zeta \rightarrow 0} Q = 1$. Other two options describe the free and evanescent (or trapped, when using Baines (1995) terminology) waves:

$$c = \begin{cases} e^{\Delta\zeta(-1/2+i\xi)}, & -1 < Q < 1, \\ e^{-\Delta\zeta(1/2+q)}, & Q > 1, \end{cases} \quad (13)$$

where

$$q = \frac{\ln(Q + \sqrt{Q^2 - 1})}{\Delta\zeta}, \quad \xi = \frac{1}{\Delta\zeta} \cdot \begin{cases} \arctan \frac{\sqrt{1-Q^2}}{Q}, & Q > 0, \\ \pi/2, & Q = 0, \\ \pi - \arctan \frac{\sqrt{1-Q^2}}{|Q|}, & Q < 0. \end{cases} \quad (14)$$

The discrete solution (8) becomes in case of decrease factor (13)

$$\omega_{j+1/2} = \omega_{1/2} \cdot \begin{cases} e^{j\Delta\zeta(-1/2+i\xi)}, & -1 < Q < 1, \\ e^{-j\Delta\zeta(1/2+q)}, & Q > 1, \end{cases} \quad (15)$$

which presents the discrete approximation to the exact solution (5). If

$$\Delta\zeta \ll 1, \quad (16)$$

which presents the vertically high-resolution case, then

$$Q \approx 1 + \frac{\Delta\zeta^2}{2} \left(\frac{1}{4} - \lambda \right).$$

If, in addition,

$$\left| \frac{\Delta\zeta^2}{2} \left(\frac{1}{4} - \lambda \right) \right| \ll 1, \quad (17)$$

then

$$q \rightarrow \sqrt{1/4 - \lambda}, \quad \xi \rightarrow \sqrt{\lambda - 1/4},$$

and the discrete approximation (15) will merge to exact solution (5).

Due to exponential decay of solution (15) with height, the top boundary condition (7) holds, indeed.

4.2 Recurrence initialization in non-homogenous case

We can always assume, that there is a homogeneous, inviscid layer in the top with stratification parameters, corresponding to the topmost discrete layer with index $j = M$:

$$\Delta\zeta = \Delta\zeta_M, \quad \mathbf{U} = \mathbf{U}_M, \quad T^0 = T_M^0 \rightarrow \lambda = \lambda_{\mathbf{k},M}.$$

The starting value c_M of the decrease factor in recurrence (9) can be chosen then as the decrease factor of this homogeneous top layer

$$c_M = c \quad \text{from (13), (14) .}$$

4.3 Requirements to vertical resolution

In the high vertical resolution case (16), the decrease factors c_i are supposed to be, and L^\pm are, close to unit by absolute value, yielding a constriction to the free term in (9)

$$\Delta\zeta_{i+1/2}^2 |\lambda_{i+1/2}| \ll 1 \quad (18)$$

(rather close to the condition (17)). In the case of inviscid atmosphere, $\lambda_{j+1/2}$ can become infinite for critical wave-vectors \mathbf{k}^* (specific for each level i), for which $\nu_i^2 - f^2 = (\mathbf{k}^* \cdot \mathbf{U}_i)^2 - f^2 = 0$, yielding $\Delta\zeta_{i+1/2} \rightarrow 0$ in (18). Due to discrete nature, the wave-vectors are not (except the case of the special choice of \mathbf{U}_i) strictly critical, but a lot of them can be nearly critical, $(\mathbf{k}^* \cdot \mathbf{U}_i)^2 - f^2 \approx 0$, which would cause very large λ and unfeasibly small $\Delta\zeta$. Especially sizable for numerical solution accuracy are levels with evanescent wind $\mathbf{U} \rightarrow 0$, as the corresponding critical wave-vectors are located in the maximum area of spectral amplitudes. The levels near the evanescent wind $U_i \rightarrow 0$ are called therefore as the critical layer. As numerical experimentation shows, critical layer forms at levels where $|\mathbf{U}_i| < 1 - 1.5 \text{ m/s}$. In the case of inviscid atmosphere, it is impossible to satisfy (18) for any computationally

considerable size of $\Delta\zeta$ in the critical layer. Fortunately, introduction even of a rather moderate turbulent friction would regularize λ , as $\nu_i^2 - f^2 = (\mathbf{k} \cdot \mathbf{U}_i + i\gamma k^2)^2 - f^2$ can't become zero nowhere anymore.

Using in the vicinity of critical wave-vectors an approximation $\lambda \sim k^2 H^2 N^2 / (\nu^2 - f^2)$, (18) gives

$$\Delta\zeta_{i+1/2} < \frac{1}{\sqrt{|\lambda_{i+1/2}|}} \approx \frac{\sqrt{|\nu_{i+1/2}^2 - f^2|}}{k H_{i+1/2} N_{i+1/2}}.$$

Minimization of the square-root here with respect to $\mathbf{k} \cdot \mathbf{U}$,

$\min_{-\infty < \mathbf{k} \cdot \mathbf{U} < \infty} \sqrt{|\nu_{i+1/2}^2 - f^2|} = k \sqrt{2\gamma_{i+1/2} f}$, provides an estimation for maximum vertical grid-step

$$\Delta\zeta_{i+1/2} < \frac{\sqrt{2f\gamma_{i+1/2}}}{H_{i+1/2} N_{i+1/2}}, \quad (19)$$

which is independent of horizontal wave-vector \mathbf{k} and thus, presents an 'global' estimate, enabling accurate solution for all horizontal spectral modes.

It is convenient to present the diffusion coefficient as

$$\gamma_{i+1/2} = \gamma_{i+1/2}^0 N_{i+1/2} \Delta x^2 / 2 \quad (20)$$

Nondimensional parameter $\gamma_{i+1/2}^0$ has simple sense: $1/\gamma_{i+1/2}^0$ is the e-fold decrease period in units $1/N$ for the highest horizontally resolved gravity wave mode with scale $\sim \Delta x$. In the discrete case, Δx is the horizontal

grid-step; in the horizontally continuous formalism, Δx can be estimated as the internal spatial scale of orography. From (19) and (20) we get finally

$$\Delta\zeta_{i+1/2} < \frac{\Delta x}{H_{i+1/2}} \sqrt{\gamma_{i+1/2}^0 f / N_{i+1/2}}. \quad (21)$$

As an instant, $\Delta z = H\Delta\zeta < 10$ m for $\Delta x = 1$ km, $\gamma^0 = 10^{-2}$, $f/N = 10^{-2}$. This vertical resolution limit decreases to 1 m for the ten times higher horizontal resolution $\Delta x = 100$ m.

Condition (21) should not be interpreted as an exact upper limit, but rather as a rough estimation of possible realistic vertical resolution, which are expected to provide required solution accuracy. The actual vertical resolution, though based on estimation (21), must be established experimentally in every particular case. As an example, in the horizontally one-dimensional flow experiments with critical layers, the vertical grid-step has to be taken up to ten times smaller of estimation (21) inside of a critical layer and can be chosen several times larger of (21) far away of such layer. In many cases with large by absolute value wind and moderate horizontal resolution ($\Delta x \geq 1$ km), no friction is required at all (though the friction inclusion is actually not prohibited but rather wanted as bringing model closer to reality).

5 Modeling examples

In following examples, horizontally discrete Fourier transform is applied to orography, which is presented by the 'witch of Agnesi' profile

$$h(x, y) = \frac{h_0}{1 + (x - x_0)^2/a_x^2 + (y - y_0)^2/a_y^2},$$

where the maximum height h_0 , center coordinates x_0, y_0 , and half-widths in directions of coordinate axes a_x, a_y are constant parameters. The spectral wave equation is solved using the above-described solution-factorization approach, and the result is then inverted back to physical space. Vertical velocity $w = -H\omega/p$ is shown in all examples.

Figure 1 presents the wave pattern of w for one-dimensional Agnesi ridge with $h_0 = 100$ m, $a_x = 2$ km, $a_y = \infty$. Reference temperature $T^0(p)$ presents a climatological profile (280 K on surface, lapse rate 6.5 K/km in the troposphere, and constant 202 K in the stratosphere). The unidirectional wind equals $U_x = 12$ m/s on the surface, has shear 0.25 m/s/km in the troposphere, and becomes constant $U_x = 15$ m/s in the stratosphere. The tropopause height is 12 km. Horizontal resolution is $\Delta x = 500$ m, grid-size in x-direction is 2048 points. Vertical resolution is chosen $\Delta z = 100$ m, ($\Delta\zeta \approx 0.01$), and $M = 300$ levels, while the atmosphere is inviscid with $\gamma^0 = 0$ on all levels. Control experiment shows, that vertical resolution increase and introduction of weak ($\gamma^0 = 0.01$) viscosity does not alter modeling results. However, more

strong friction with $\gamma^0 = 0.05$ would dump the wave-field moderately.

Though the buoyancy wave reflection on the tropopause and tropospheric wave-guide formation has theoretically proved some time ago (Eliassen 1968) there has been few numerical experimentation, showing the details of the process. As seen in Fig. 1. already a rather moderate tropospheric wind shear will cause substantial wave reflection on the tropopause and wave train creation (As it proves, existence of thermal tropopause alone, without positive wind shear in the troposphere, is insufficient for wave-guide formation). The wave train will increase in length with the wind shear increase and can reach several thousands kilometers (depending on the turbulent friction intensity) in length. The current example presents special interest by the wave-train wiggling, which is observable at weak shear and would disappear with shear strengthening.

Fig. 2. presents a flow over Agnesi ridge with $h_0 = 100$ m, $a_x = 3$ km, $a_y = \infty$ and with the same temperature profile as in the previous case. However, the wind is backing with height in this model, having value 10 m s^{-1} on the surface and decreasing with height linearly. It becomes zero on 5 km (Fig. 2a) and 2.5 km (Fig. 2b) levels, which perform central heights of respective critical layers, and retards with height further to constant value -2.0 m s^{-1} on 5.5 and 3 km heights, approximately. Horizontal resolution is 500 m, the number of horizontal grid-points is 256. Vertical grid-step decreases linearly with height from $\Delta z = 100$ m on the surface to $\Delta z = 5$ m on the wind reversal level, in the case of Fig. 2a, and from $\Delta z = 50$ m on the surface to

$\Delta z = 10$ m, in the case of Fig. 2b. Above these levels, the vertical grid-step is kept constant, i.e., 5 and 10 m, respectively. The number of vertical levels $M = 240$, turbulent viscosity $\gamma^0 = 0.05$.

The main aim of these examples is to demonstrate the requirements to enhanced resolution in vicinity of critical layer. The coincidence with earlier reported results (Miranda and Valente 1997, Grubišić and Smolarkiewicz 1997, Shen and Lin 1999, Shutts and Gadian 1999), is excellent, demonstrating complete absorption of scattered from orography waves in the critical layer.

Fig. 3. shows horizontal cross-sections of w at different heights for a wind, sheared both by amplitude and direction, blowing over a circular hill with $h_0 = 300$ m, $a_x = a_y = 3$ km. Horizontal resolution is $\Delta x = \Delta_y = 1.1$ km, horizontal grid consists of 256x256 points. The model has 300 levels with constant resolution $\Delta z = 50$ m in vertical. The turbulent viscosity $\gamma^0 = 0.05$. The reference atmosphere is isothermal with $T^0 = 280$ K. The wind amplitude is a hyperbolic function of height with maximum 40 m/s at $z = 15$ km, while wind direction rotates uniformly with the height:

$$u_x = U(z)\cos(\pi z/z_{rev}), \quad u_y = U(z)\sin(\pi z/z_{rev}), \quad z_{rev} = 12km,$$

$$U(z) = U_s + U_0 \left(1 - \frac{z}{z_{max}}\right) \frac{z}{z_{max}}, \quad U_s = 10m/s, \quad U_0 = 120m/s, \quad z_{max} = 30km.$$

Solution is insensible to vertical resolution doubling, which means, that constant resolution $\Delta z = 50$ m is sufficient here. However, the decrease of γ^0 to

0.01 forces a complementary vertical grid-step decrease to $\Delta z = 20$ m.

The qualitative coincidence of the present example with former analytical (Shutts 1998, 2003) and numerical (Grubišić and Smolarkiewicz 1997) results is excellent, though a quantitative comparison is not available in analytical case, as models with such a wind complexity are not solved analytically yet. The typical feature of this kind of flow regimes with uniform directional wind shear is the complete buoyancy wave absorption to the wind reversal height

z_{rev} .

6 Conclusions

The described solution factorization method presents adequate, simple and fast for orographic wave modeling in the case of rather sophisticated flow regimes both in spatially two- and three dimensional cases. Experiments with realistic height-dependent temperature, including the tropopause, and optional sheared winds are attainable. Rather large modeling domains in association with high horizontal and vertical resolutions can be used, which makes high-resolution modeling of extended wave-fields possible. As an example, in horizontally one-dimensional case, horizontal domain of 5000 km lengths with 500 m horizontal resolution and 1000 levels in vertical with 10 m vertical resolution would be ordinary computational task for a PC.

The requirement for vertical resolution (21) holds good, if the reference wind does not become evanescent on some height. As numerical experimentation

shows, for large by absolute value winds ($U = 10$ m/s can be considered 'large') and for moderate horizontal resolutions ($\Delta z \geq 1$ km), the inviscid atmospheric model can even be used without loss of stability and accuracy. However, wind evanescence on some level, associated with formation of a critical layer around that height, will require quite high vertical resolutions (up to $\Delta z \sim 1$ m at horizontal resolutions $\Delta x \sim 100$ m), in the vicinity and inside of the critical layer, outmatching resolution condition (21) about 5 to 10 times. The extremely high requirement for resolution turns modeling of critical layer events to a most expensive and resource-demanding computational tasks.

The area of application of the developed numerical solution is high resolution, high precision modeling of orographic waves for arbitrary orography in complex atmospheric stratification conditions. The model can be applied also as a test-tool for numerical accuracy checking of adiabatic kernels of the nonlinear nonhydrostatic NWP models.

Acknowledgments

This investigation has been supported by Estonian Science Foundation under Research Grant 5711.

7 References

- Baines, P. G., 1995: *Topographic Effects in Stratified Flows*. Cambridge Univ. Press, 482 pp.
- Berkshire, F. H., 1975: Critical levels in a three-dimensional stratified shear flow. *Pure Appl. Geophys.*, **113**, 561 - 568.
- Broad, A. S. , 1995: Linear theory of momentum fluxes in 3-D flows with the turning of the mean wind with height. *Q. J. R. Meteorol. Soc.*, **121**, 1891 - 1902.
- Broad, A. S. , 1999: Do orographic gravity waves break in flows with uniform wind direction with height? *Q. J. R. Meteorol. Soc.*, **125** 195 - 1714.
- Broutman, D. , Rottman, J. W. , Eckermann, S. D., 2003: A simplified Fourier method for nonhydrostatic mountain waves *J. Atmos. Sci.*, **60**, 2686 - 2696.
- Clark, T. L.,1977: A small-scale dynamic model using a terrain following coordinate transformation. *J. Comput. Phys.*, **24**, 186 – 215.
- Crapper, G. D., 1959: A three-dimensional solution for waves in the lee of mountains. *J. Fluid Mech.*, **6**, 51 -76.
- Crapper, G. D., 1962: Waves in the lee of mountain with elliptical contours. *Philos. Trans. Roy. Soc. London*, **254A**, 601 - 623.
- Drazin, P., G., D. W. Moore, 1967: Steady two-dimensional flow of fluid of variable density over an obstacle. *J. Fluid Mech.*, **28**, 353 – 370.

- Durran, D. R., and J. B. Klemp, 1983: A compressible model for the simulation of moist mountain waves. *Mon. Weather Rev.*, **111**, 2341 – 2361.
- Eliassen, A., 1968: On the meso-scale mountain waves on the rotating Earth. *Geofys. Publicasjoner*, **27**, No 6, 1 - 15.
- Gjevik, B., T. Marthinsen, 1978: Three-dimensional lee-wave pattern. *Q. J. R. Meteorol. Soc.*, **104**, 947 - 957.
- Grubišić, V., P. K. Smolarkiewicz, 1997: The effect of critical levels on 3D orographic flows. Linear regime. *J. Atmos. Sci.*, **54**, 1943 - 1960.
- Hazel P., 1967: The effect of viscosity and heat conduction on internal gravity waves at a critical level. *J. Fluid Mech.*, **30**, 775 - 783.
- Holton J R, M J Alexander, 1999: Gravity waves in the mesosphere generated by tropospheric convection, *Tellus*, **51A-B**, 45-58.
- Janovich, G.S., 1984: Lee waves in three-dimensional stratified flow. *J. Fluid Mech.*, **148**, 97 - 108.
- Jones, W. L., 1967: Propagation of internal gravity waves in fluids with shear flow and rotation. *J. Fluid Mech.*, **30**, 439 - 488.
- Klemp, J. B., and D. K. Lilly, 1978: Numerical simulation of hydrostatic mountain waves. *J. Atmos. Sci.*, **35**, 78 – 107.
- Laprise R., and W. R. Peltier, 1989: On the structural characteristics of steady finite-amplitude mountain waves over bell-shaped topography. *J. Atmos. Sci.*, **46** 586 – 595.
- Lin, C. C., 1955: *The Theory of Hydrodynamic Instability*. Cambridge: Cam-

bridge Univ. Press.

Long, R. R., 1953: Some aspects of the flow of stratified fluids. Part I: A theoretical investigation. *Tellus*, **5**, 42 – 58.

Long, R. R., 1954: Some aspects of the flow of stratified fluids. Part II: Experiments with a two fluids system. *Tellus*, **6**, 97 – 115.

Männik, A., R. Rõõm, A. Luhamaa, 2003: Nonhydrostatic generalization of a pressure-coordinate-based hydrostatic model with implementation in HIRLAM: validation of adiabatic core. *Tellus*, **55A**, 219 – 231.

Miles J. W., 1968a: Lee waves in a stratified flow. Part 1. Thin barrier. *J. Fluid Mech.*, **32**, 549 - 567.

Miles J. W., 1968b: Lee waves in a stratified flow. Part 2. Semi-circular obstacle. *J. Fluid Mech.*, **33**, 803 - 814.

Miles J. W., and H. E. Hupert, 1969: Lee waves in a stratified flow. Part 4. Perturbation approximations. *J. Fluid Mech.*, **35**, 481 – 496.

Miller, M. J., 1974: On the use of pressure as vertical co-ordinate in modelling convection. *Q. J. R. Meteorol. Soc.*, **100**, 155 – 162.

Miller, M. J., R. P. Pearce, 1974: A three-dimensional primitive equation model of cumulonimbus convection. *Q. J. R. Meteorol. Soc.*, **100**, 133 – 154.

Miller, M. J., A.A. White, 1984: On the nonhydrostatic equations in pressure and sigma coordinates. *Q. J. R. Meteorol. Soc.*, **110**, 515 – 533.

Miranda, P. M. A., I. N. James, 1992: Non-linear three-dimensional effects on

- gravity-wave drag. Splitting flow and breaking waves. *Q. J. R. Meteorol. Soc.* **118**, 1057 – 1081.
- Miranda P.M.A., M.A. Valente, 1997: Critical level resonance in three-dimensional flow past isolated mountains. *J. Atmos. Sci.*, **54**, 1574 – 1588.
- Nance, L. B., Durran, D. R., 1997: A modeling study of nonstationary trapped mountain lee waves. Part I. Mean-flow variability. *J. Atmos. Sci.*, **55**, 2275 – 2291.
- Nance, L. B., Durran, D. R., 1998: A modeling study of nonstationary trapped mountain lee waves. Part II. Nonlinearity. *J. Atmos. Sci.*, **55**, 1429 – 1445.
- Phillips, D. S., 1984: Analytic surface pressure and drag for linear hydrostatic flow over three-dimensional elliptical mountains. *J. Atmos. Sci.*, **41**, 1073 - 1084.
- Pinty, J.-P., Benoit, R., Richard, E., Laprise, R., 1995: Simple tests of a semi-implicit semi-Lagrangian model on 2D mountain wave problems. *Mon. Weather Rev.*, **123**, 3042 – 3058.
- Polvani L M, Scott R K Thomas S J 2004: Numerically converged solutions of the Global primitive equations for testing the dynamical core of atmospheric GCMs. *Mon. Weather Rev.*, **132**, 2539 - 2552.
- Queney, P., 1948: The problem of airflow over mountains. a summary of theoretical studies. *Bull. Amer. Met. Soc.*, **29**, 16 – 26.
- Rõõm, R., 1998: Acoustic filtering in nonhydrostatic pressure-coordinate

- dynamics: A variational approach. *J. Atmos. Sci.*, **55**, 654 - 668.
- Rõõm, R., Männik, A., 1999: Response of different nonhydrostatic, pressure-coordinate models to orographic forcing. *J. Atmos. Sci.*, **56**, 2553–2578.
- Rõõm, R., Miranda P. M. A, Thorpe, A. J., 2001: Filtered non-hydrostatic models in pressure-related coordinates. *Q. J. R. Meteorol. Soc.*, **127**, 1277-1292 .
- Rõõm, R., Männik, A. and Luhamaa, A. 2006: Nonhydrostatic adiabatic kernel for HIRLAM. Part IV: Semi-implicit Semi-Lagrangian scheme. *HIRLAM Technical Report*, **65**, 43 p. Available from <http://hirlam.org/open/publications/TechReports/TR65.pdf>
- Rottman, J. W., D. Broutman, R. Grimshaw, 1996: Numerical simulation of Uniformly stratified flow over topography. *J. Fluid Mech.*, **306**, 1 - 30.
- Saito, K., Dohms, G., Schaettler, U., Steppeler, J., 1998: 3-D mountain waves by the Lokal-Modell of DWD and the MRI Mesoscale Nonhydrostatic Model. In. *SRNWP-Centre for Nonhydrostatic Modeling, Newsletter No. 2*, DWD GB FE, Offenbach, February 1998, **3** – 13.
- Scorer, R. S., 1949: Theory of waves in the lee of mountains. *Q. J. R. Meteorol. Soc.*, **75**, 41 – 56.
- Sharman, R. D., M. G. Wurtele, 1983: Ship waves and lee waves. *J. Atmos. Sci.*, **75**, 41 - 56.
- Sharman, R. D., M G Wurtele, 2004: Three-dimensional structure of forced gravity waves and lee waves. *J. Atmos. Sci.*, **61**, 664 - 681.

- Shen, Bo-Wen; Lin, Yuh-Lang. 1999: Effects of Critical Levels on Two-Dimensional Back-Sheared Flow Over an Isolated Mountain Ridge . *J. Atmos. Sci.*, **56**, 3286 - 3302.
- Shutts, G. J., 1995: Gravity-wave drag parameterization over complex terrain. The effect of critical level absorption in directional wind shear. *Q. J. R. Meteorol. Soc.*, **121**, 1005 - 1021.
- Shutts, G. J., 1998: Stationary gravity wave structure in flows with directional wind shear. *Q. J. R. Meteorol. Soc.*, **124**, 1421 - 1442.
- Shutts G, J., 2003: Inertia-gravity wave and neutral Eady wave trains forced by directionally sheared flow over isolated hills. *J. Atmos. Sci.*, **60** , 593 - 606.
- Shutts, G. J., and A. Gadian, 1999: Numerical simulations of orographic gravity waves in flows which back with height. *Q. J. R. Meteorol. Soc.*, **125**, 2743 - 2765.
- Smith, R. B., 1980: Linear theory of stratified hydrostatic flows past an isolated mountain. *Tellus*, **32**, 348 - 364.
- Smith, R. B., 1988: Linear theory of stratified flow past an isolated mountain in isosteric coordinates. *J. Atmos. Sci.*, **45**, 3889 - 3896.
- Smith, R. B., 1989a: Mountains induced stagnation points in hydrostatic flow. *Tellus*, **41A**, 270 - 274.
- Smith, R. B., 1989b: Hydrostatic airflow over mountains. *Advances in Geophysics*, **31**, Academic press, 1 - 41.

- Teixeira M. A. C., Miranda P. M. A, 2004: The effect of wind shear and curvature on the gravity wave drag. *J. Atmos. Sci.*, **61**, 2638 – 2643.
- Welch W T, Smolarkiewitz, P., 2001: The large-scale effects of flow over periodic mesoscale topography. *J. Atmos. Sci.*, **58**, 1477 - 1492.
- White, A. A. ,1989: An extended version of nonhydrostatic, pressure coordinate model. QJRMS115, 1243 – 1251.
- Wurtele M. G. , 1957: The three-dimensional lee wave. Beitr. Phys. Atmos., **29** 242 - 252.
- Wurtele, M. G., R. D. Sharman and T. L. Keller, 1987: Analysis and simulations of a troposphere-stratosphere gravity wave model. Part I. *J. Atmos. Sci.*, **44**, 3269 – 3281.
- Wurtele, M. G., A. Datta, and R. D. Sharman, 1996: The propagation of gravity-inertia waves and lee waves under a critical level. *J. Atmos. Sci.*, **53**, 1505 – 1523.
- Xue, M., A. J. Thorpe, 1991: A mesoscale numerical model using the nonhydrostatic pressure-based sigma-coordinate equations. Model experiments with dry mountain flows. *Month. Wea. Rev.*, **119**, 1168 – 1185.

Figure Captions

Fig. 1 Vertical velocity waves in the case of Agnesi ridge with 100 m height and 2 km half-width for constant temperature lapse rate 6.5 K/km and constant unidirectional wind shear $0.25 \text{ m s}^{-1} \text{ km}^{-1}$ in the troposphere. Tropopause height is 12 km. Interval between isotachs $\Delta w = 0.1 \text{ m s}^{-1}$.

Fig. 2 Vertical cross-section of the vertical wind for flow over Agnesi ridge with $h = 100 \text{ m}$, $a_x = 2 \text{ km}$. The surface wind is 10 m/s, wind is unidirectional, backing with height evenly and reaching zero on the critical height $z_{cr} = 5 \text{ km}$ (a) and 2.5 km (b). Interval between isotachs $\Delta w = 0.05 \text{ m s}^{-1}$.

Fig. 3 Horizontal cross-section of vertical wind at heights (a) 1 km, (b) 4 km, (c) 7 km and (d) 9 km. Circular hill with 300 m height and 3 km half-width is located at $x = y = 100 \text{ km}$. Atmosphere is isothermal with $T = 280 \text{ K}$. Reference wind profile $|\mathbf{U}|$ is hyperbolic, with minimum value 10 m/s at surface and maximum value 40 m/s at $z = 15 \text{ km}$. Wind, blowing on surface to east (along x-axis), turns with height evenly counterclockwise, changing direction to opposite on the height $z = 12 \text{ km}$. Isotachs are drawn with 0.2 m/s interval.

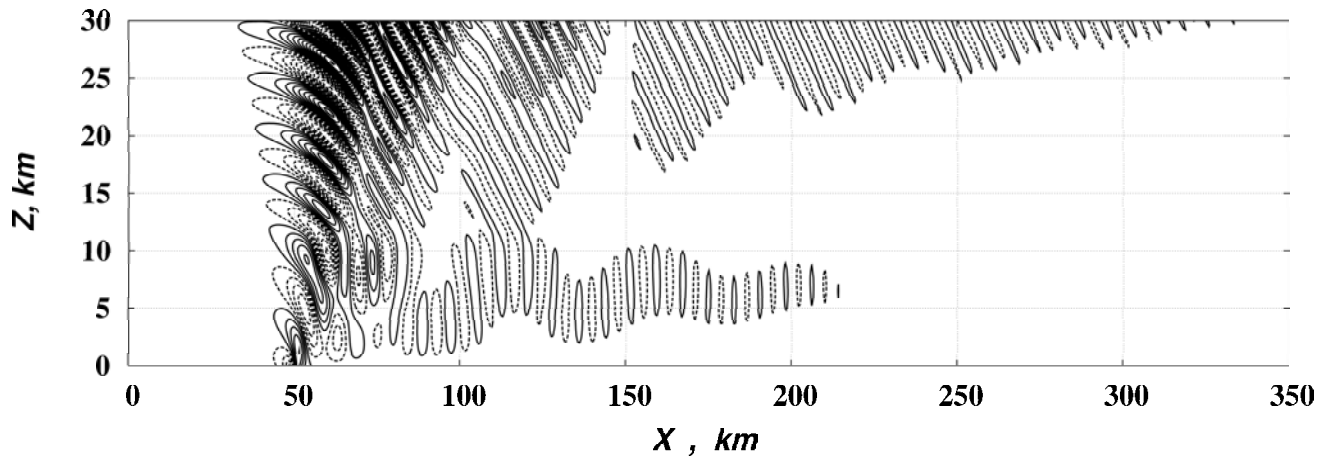


Fig. 1 Vertical velocity waves in the case of Agnesi ridge with 100 m height and 2 km half-width for constant temperature lapse rate 6.5 K/km and constant unidirectional wind shear $0.25 \text{ m s}^{-1} \text{ km}^{-1}$ in the troposphere. Tropopause height is 12 km. Interval between isotachs $\Delta w = 0.1 \text{ m s}^{-1}$.

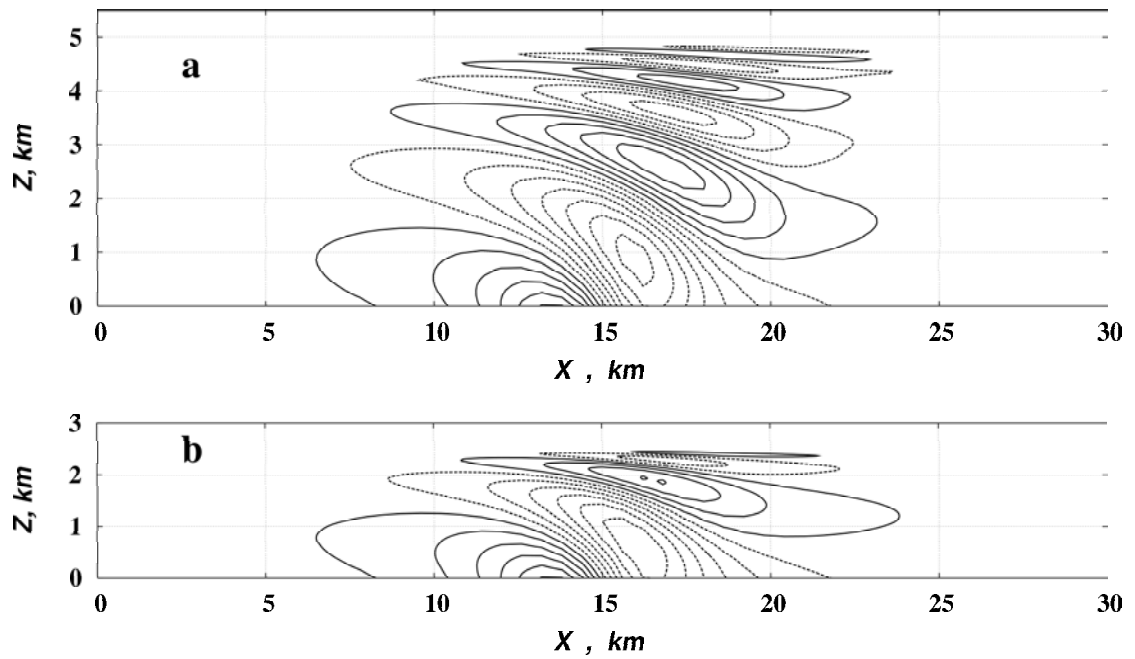


Fig. 2 Vertical cross-section of the vertical wind for flow over Agnesi ridge with $h = 100$ m, $a_x = 2$ km. The surface wind is 10 m/s, wind is unidirectional, backing with height evenly and reaching zero on the critical height $z_{cr} = 5$ km (a) and 2.5 km (b). Interval between isotachs $\Delta w = 0.05$ $m s^{-1}$.

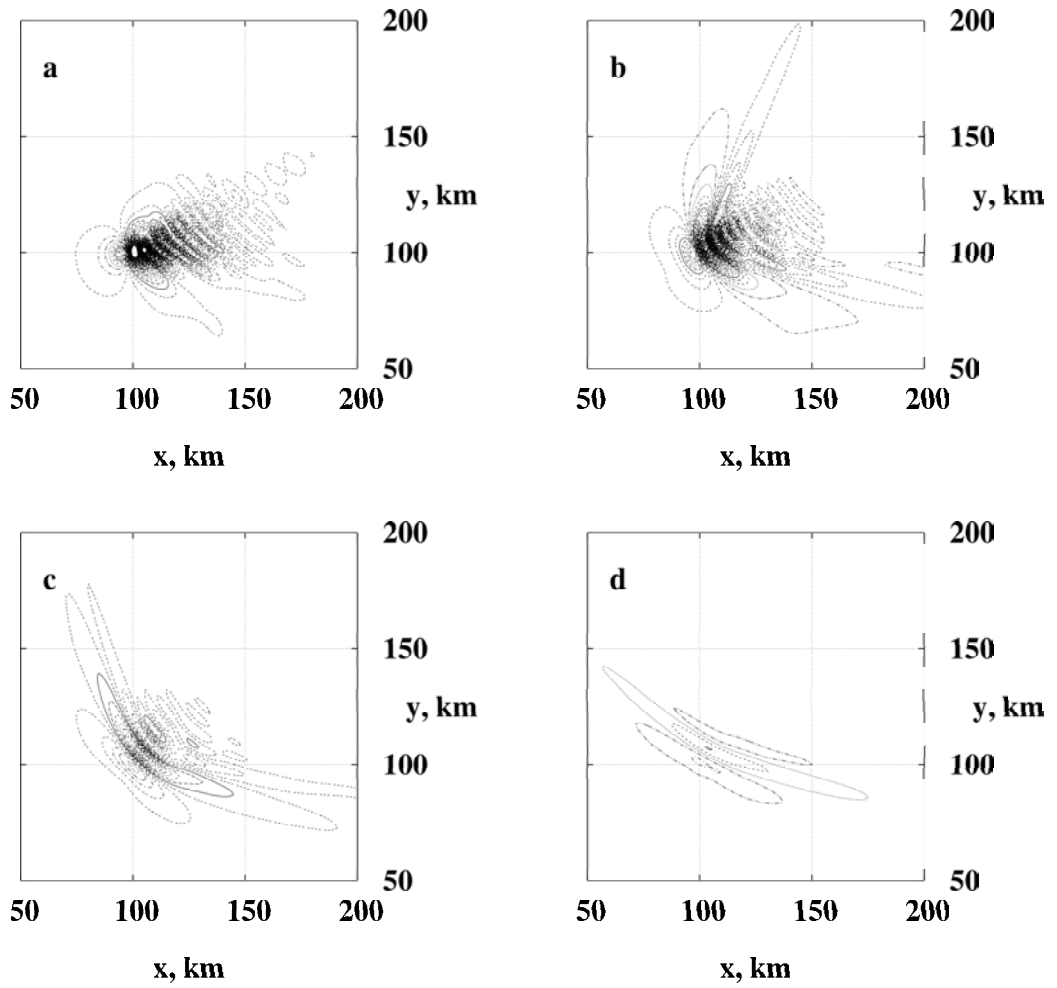


Fig. 3 Horizontal cross-section of vertical wind at heights (a) 1 km, (b) 4 km, (c) 7 km and (d) 9 km. Circular hill with 300 m height and 3 km half-width is located at $x = y = 100$ km. Atmosphere is isothermal with $T = 280$ K. Reference wind profile $|\mathbf{U}|$ is hyperbolic, with minimum value 10 m/s at surface and maximum value 40 m/s at $z = 15$ km. Wind, blowing on surface to east (along x-axis), turns with height evenly counterclockwise, changing direction to opposite on the height $z = 12$ km. Isotachs are drawn with 0.2 m/s interval.